

Article

Novel Synthesis of Core-Shell Biomaterials from Polymeric Filaments with a Bioceramic Coating for Biomedical Applications

Catalina-Andreea Dascalu ¹, Florin Miculescu ^{1,*} , Aura-Catalina Mocanu ¹,
Andreea Elena Constantinescu ¹, Tudor Mihai Butte ¹, Andreea Madalina Pandeale ^{2,3},
Robert-Catalin Ciocoiu ¹ , Stefan Ioan Voicu ²  and Lucian Toma Ciocan ⁴

¹ Department of Metallic Materials Science, Physical Metallurgy, University Politehnica of Bucharest, 060042 Bucharest, Romania; catalina.dascalu@hotmail.com (C.-A.D.); mcn_aura@hotmail.com (A.-C.M.); andreeaelena01c@gmail.com (A.E.C.); butte.tudor@yahoo.com (T.M.B.); ciocoiurobert@gmail.com (R.-C.C)

² Department of Analytical Chemistry and Environmental Engineering, University Politehnica of Bucharest, 011061 Bucharest, Romania; pandele.m.a@gmail.com (A.M.P.); svoicu@gmail.com (S.I.V.)

³ Advanced Polymer Materials Group, University Politehnica of Bucharest, 011061 Bucharest, Romania

⁴ Prosthetics Technology and Dental Materials Department, University of Medicine and Pharmacy, 020022 Bucharest, Romania; tciocan@yahoo.com

* Correspondence: f_miculescu@yahoo.com; Tel.: +40-21-3169563

Received: 12 February 2020; Accepted: 15 March 2020; Published: 18 March 2020



Abstract: Bone tissue engineering is constantly in need of new material development with improved biocompatibility or mechanical features closer to those of natural bone. Other important factors are the sustainability, cost, and origin of the natural precursors involved in the technological process. This study focused on two widely used polymers in tissue engineering, namely polylactic acid (PLA) and thermoplastic polyurethane (TPU), as well as bovine-bone-derived hydroxyapatite (HA) for the manufacturing of core-shell structures. In order to embed the ceramic particles on the polymeric filaments surface, the materials were introduced in an electrical oven at various temperatures and exposure times and under various pressing forces. The obtained core-shell structures were characterized in terms of morphology and composition, and a pull-out test was used to demonstrate the particles adhesion on the polymeric filaments structure. Thermal properties (modulated temperature and exposure time) and the pressing force's influence upon HA particles' insertion degree were evaluated. More to the point, the form variation factor and the mass variation led to the optimal technological parameters for the synthesis of core-shell materials for prospect additive manufacturing and regenerative medicine applications.

Keywords: bioceramic coating; fused filament fabrication; fused deposition modelling; biogenic hydroxyapatite; core-shell structure

1. Introduction

By combining the knowledge and needs of scientists, engineers, and surgeons, the field of biomaterials is constantly expanding. Thus, daily, new biocompatible materials are developed with the sole purpose of ensuring the tissues and organs proper functioning in the human body in a safe and efficient way [1]. In the case of bone tissue defects generated by traumas or diseases, the reconstruction of its structural integrity is a long-studied problem and of current interest to the specialists [2–5].

In this light, the already reported reconstruction methods involving metallic structures, polymeric biomaterials [6,7] (such as polylactic acid (PLA), thermoplastic polyurethane (TPU), polyglycolic acid (PGA), poly (vinyl alcohol) (PVA) [1,8,9]), and ceramics (mostly hydroxyapatite) [1,10–13] are of crucial

importance. Among these, PLA was widely used, mainly due to its biocompatibility with the human organism and the advantageous synthesis alternative from sustainable natural resources (e.g., beet or maize) [14]. Along with PLA, TPU was remarked in the additive manufacturing technology [15]. The TPU applications in the medical field spread from blood vessels, implants, and prosthetics, to scaffolding in tissue engineering, dialysis membranes, or breast implants [16].

Furthermore, naturally derived hydroxyapatite (HA) is a bioactive ceramic, with similar chemical and structural properties to the mineral component of the natural bone tissue, and exceptional biocompatibility and osteoconductivity. HA can be synthesized from various renewable resources (e.g. fish, sheep, cattle or bovine bones [17,18] or marine shells [19,20]).

Along with the development of new biomaterials, the cost-efficient and highly performant processing techniques for final products manufacturing are also in need of improvement. Additive manufacturing (AM) or 3D printing can be considered 21st century technology due to the possibility to attain patient-customized and adapted products [14]. However, the most widely and accessible used technique in orthopedics is fused deposition modeling (FDM) or fused filler fabrication (FFF) [8,14,21,22], which provide 3D scaffolds with a well-defined design by extruding a digital 3D model from thermoplastic polymeric materials heated to their melting point [22].

This study aims to provide a new core-shell material that can be used in the FDM technique, targeted due to its rigorous control of parameters (temperature, bed temperature, feed rate, printing speed, etc.) [23–27].

Therefore, this study focused on the development of a completely new technique for the HA particle adhesion on PLA and TPU filaments' surface, destined for scaffolds manufacturing with applicability in both dentistry and orthopedic reconstruction surgery.

When addressing the prospect of generating a ceramic coating on a polymeric surface, two important aspects are to be considered: i) the necessity (if any) of polymeric surface features modification and ii) the involved coating technique. Dedicated studies reported several methods for polymers' surface modification, both physical (flame treatment, metal deposition, irradiation techniques and corona-discharge techniques, plasma treatment, etc.) [28–30] and chemical (wet chemical methods, surfaces treated with hydrogen peroxide, solution processing method, etc.) [28,30]. In comparison, the novelty of the proposed method described in this study relies on no modification treatment of the polymeric filaments surface prior to ceramic particles' adhesion. More to the point, in terms of coating techniques, the specialized literature pictures a wide range of simulations (e.g., the Monte Carlo method, the finite element method, etc.) [31,32] and mathematical modelling approaches [33,34] for particle coating and adhesion on different substrates, polymeric included [22,35–39]. None of these are involved whatsoever in the proposed synthesis route of the core-shell materials. Our strategy targets the formation of an osteoconductive HA shell coating through rigorous control of the synthesis key-working parameters for particle distribution and incorporation on the polymeric surface.

This leads to a tunable synthesis technology with a precise optimal range for the pressing force, thermal treatment time, and temperature applied to the core-shell materials for future compatible additive manufacturing and medical applications. In this regard, the present study followed a well-designed and complex investigation program, starting with preliminary morpho-compositional [40,41], thermogravimetric, and differential scanning calorimetry analysis, which afford the choice of the heat treatment parameters for an optimal adhesion and insertion of HA particles on the polymeric filaments. Furthermore, the implantation/adhesion degree of the HA particles and the polymeric filaments deformation degree were exposed through form factor variation and mass variation analyses. The performed mechanical tests in terms of compression resistance and pull-out analysis intend to demonstrate the similarity with the cortical bone tissue, the particle adhesion strength on the polymeric surface, and the applicability extent of these material types in the dentistry and orthopedic fields.

As a result, a complete and compatible replacement of the core-shell structures with newly formed bone tissue is expected, when implanted.

2. Materials and Methods

2.1. Core-shell Materials Synthesis

In order to obtain the core-shell structures, namely the polymer coated with bioceramic, the two types of well-known polymeric materials with acknowledged history, composition, and properties [42,43] were involved, namely PLA filament (Innofil, BASF 3D Printing Solutions BV, Emmen, Netherlands) and TPU filament (Ninja Flex, NinjaTek, Manheim, PA, USA). The diameter of both full structure filaments (not tubular) specified by the manufacturer is of 1.75 ± 0.05 mm.

The filaments were placed on a bed of bovine-bone-derived HA powder (synthesized through an established and completely reproducible method, as previously reported [44]), with a particle size of $>125 \mu\text{m}$, on top of which a new powder layer was added (necessary to completely cover the filament). HA powder was obtained after three thermal processes, one of boiling, one of deproteinization and one of calcination in electric oven, followed by grinding in ball mill and granulometric sorting [20,45,46].

The soaked filaments were pressed under the action of different pressing forces (see Figure 1 and Table 1). The next step involved the thermal treatment of these samples into an electrical oven for different periods of time (30', 60', and 120') and different temperatures (195, 205, and 215 °C). These temperatures were chosen based on the working temperatures range of 3D printers [47,48] and following the thermo-gravimetric and differential scanning calorimetric analysis of the polymeric filaments. The last step involved the ultrasonic vibration of the samples in order to remove the particles that did not adhere to the polymers' surface. Due to the small size of the filaments, a high embedding degree was necessary in order to obtain a good accuracy of the results.

The modification of the technological parameters, namely the pressing force, time, and temperature, has a direct influence on the final coating morphology, as can be seen in Figure 1 below.

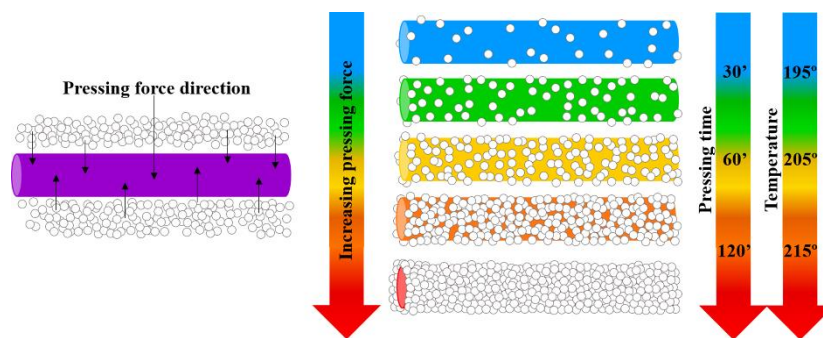


Figure 1. Schematic influence of the synthesis parameters on the final bioceramic coating.

Based on the aforementioned technological synthesis process, the samples' denomination was performed according to Table 1 below.

Table 1. Samples' denomination according to synthesis parameters.

Sample Type	Pressing Force [MPa]	Thermal Treatment	
		Exposure Time [min]*	Temperature [°C]*
Reference	0		
0.5×10^{-4} MPa	0.5×10^{-4}	30	195
1.5×10^{-4} MPa	1.5×10^{-4}	60	205
2.5×10^{-4} MPa	2.5×10^{-4}	120	215
5×10^{-4} MPa	5×10^{-4}		

* parameters applied for each pressing force.

All technological synthesis and investigation stages were performed in the laboratories of the University Politehnica of Bucharest on calibrated equipment; the experimental data were acquired through calibrated software, and, for all the quantitative results, the standard deviation was graphically disclosed.

2.2. Characterization Techniques

The morpho-compositional evaluation of the core-shell samples on both surface and cross-section and the degree of ceramic particle incorporation were determined by scanning electron microscopy (SEM) with a Philips XL 30 ESEM TMP microscope (FEI/Phillips, Hillsboro, OR, USA) equipped with an auxiliary energy dispersive spectrometer (EDAX Sapphire UTW). To achieve the micrographs, an acceleration voltage of 25 kV and a 10-mm working distance was used. The investigations were performed in five randomly chosen areas. Compositional analysis is an additional indicator regarding the ceramic/polymer ratio in the sample surface.

Thermo-gravimetric analysis was performed on a Q500 equipment (TA Instruments, New Castle, DE, SUA), in air atmosphere, at temperatures between 20–350 °C and a heating rate of 10 °C/min. The differential scanning calorimetric analysis was performed on a Netzch Proetus equipment (TA Instruments, New Castle, DE, SUA), in air atmosphere, at temperatures between 20–350 °C and a heating rate of 10 °C/min.

The TGA/differential scanning calorimetry (DSC) analysis was imperative for choosing the appropriate heat treatment program.

Mass variation was performed on a calibrated four decimal analytical balance (Kern and Sohn GmbH, Balingen, Germany) before and after the filaments' embedment in HA powder.

The compression test was performed using a universal test machine Walter + Bai AG, Loehningen (Schaffhausen, Switzerland), type LfV300. The used test speed was 1 mm/min with an acquisition rate of 0.01 s. The measurements were performed in triplicate.

The pull-out test was performed using the same universal test machine Walter + Bai AG, Loehningen (Schaffhausen, Switzerland), type LfV300. The samples were requested in traction by moving the crossbar with a speed of 5 mm/min. The measurements were performed on five samples from each core-shell material type. The test was performed by adapting the procedure of ASTM C633-13 "Standard test method for adhesion or cohesion strength of thermal spray coatings" [49] to the dimensions of the obtained samples, i.e., core-shell materials with a 2-mm average diameter (as can be seen in Figure S1 in the Supplementary Material). Thus, for fixing the filaments, a 2-mm diameter steel rod was used, and the surface in contact with the adhesive was processed in the same way for all the rods in order to ensure the reproducibility and repeatability of the test. In the specialized literature, the epoxy adhesive [29,50–54] is most often encountered for such applications, but it was considered to be inadequate due to the mechanical characteristics (elasticity of approx. 35 GPa), as compared to PLA (approx. 3.5 GPa) and TPU (approx. 2.5 GPa), which would lead to a non-uniform state of deformations (the polymers would be more intensely deformed and could yield before the joint). In this light, the chosen adhesive for our particular study is a cyanoacrylate (Fenedur, Montevideo, Uruguay) with an elasticity modulus of approx. 1.3 GPa, which was previously reported in applications destined for different medical fields (orthopedics, plastic surgery, dermatology, etc.) [55].

3. Results and Discussion

3.1. Morpho-compositional Characterization

The present research involved preliminary studies on PLA and TPU filaments with modified core (polymer)–shell (ceramic) structure. These studies were based on morpho-compositional analysis, given that coating morphology is a must-criteria and the most important factor for the targeted materials along with chemical composition [44].

In terms of morphology, the differences between samples can be clearly observed. The temperature is the main factor that influenced the samples' morphology, as illustrated in Figure 2.

At 195 °C, different amounts of small sized particles adhered to the surface of both polymeric materials: a larger quantity of particles generated a rougher appearance of the PLA filaments surface, as compared to a lower degree in the case of TPU samples, which led to a smoother surface with a roughly uniform distribution.

As the temperature increases, a change in the coating morphology is observed, so that at 205 °C, both small and large particles' dimensions adhered to the surface of both polymers. In the case of the PLA filament, small particles adhered to the polymeric surface, whereas in the case of TPU, the predominance is attributed to the particles in the upper dimension range of the HA powder type used.

The maximum temperature used in this study (215 °C) has a defining influence on the appearance of the materials' coatings, so that, on the surface of both types of polymers, only large particles ultimately adhered.

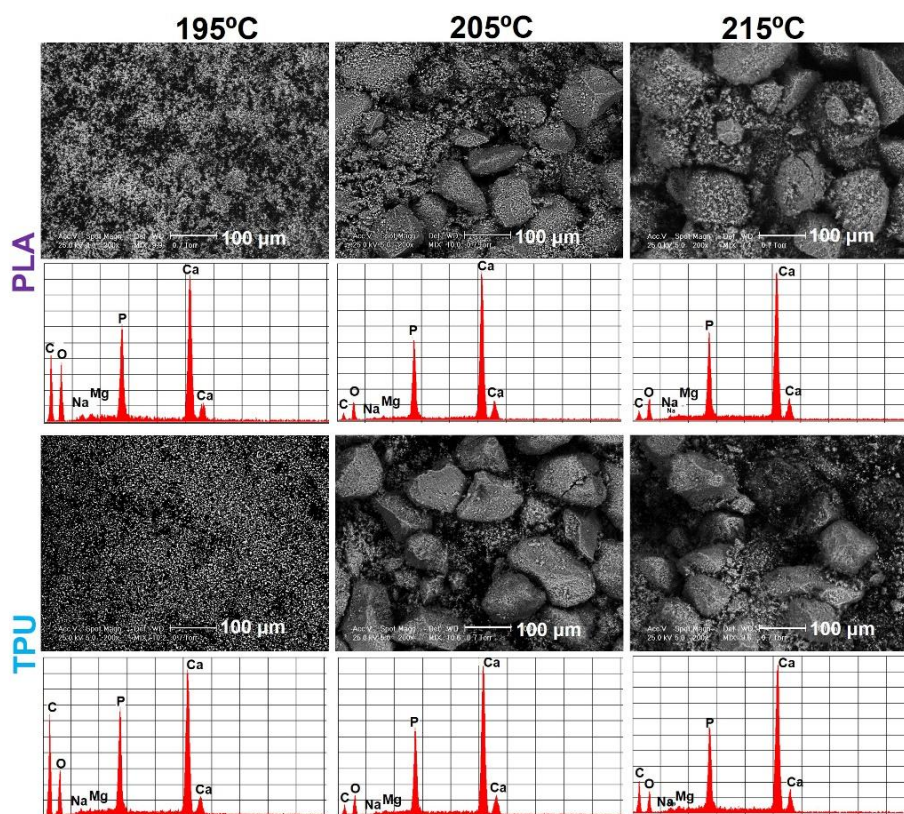


Figure 2. Preliminary morpho-compositional characterization of polylactic acid (PLA) and thermoplastic polyurethane (TPU) polymer coated with hydroxyapatite (HA) particles at 195, 205, and 215 °C.

Regarding the compositional analysis, the EDS (Energy-Dispersive X-ray Spectroscopy) spectra of both polymer types revealed specific peaks of the HA main elements, especially Ca and P [44]. The presence of the carbon peak in the spectra denotes the existence of the polymeric substrate.

Thus, at 195 °C, the intensity of the carbon peak is high, which supports the morphological investigations that have shown the addition of the small particles and the presence of the polymer between them. In addition, as mentioned above, a clear difference can be observed between the PLA and TPU filament regarding carbon peak intensity. In the case of the first polymer, several particles adhered to its surface; therefore, a higher degree of surface coverage determined a low carbon peak intensity. As the temperature rises to 205 °C, the intensity of the carbon peak drops drastically, and stands as proof of the addition of a large number of particles to the surface of the polymer, and thus a high degree of coverage.

Further increased temperature up to 215 °C generates changes in the compositional analysis of the samples. The carbon peak intensities begin to increase (compared to the temperature of 205 °C), this phenomenon being attributed to the fact that at elevated temperatures the polymer infiltrates between particles and incorporates them.

3.2. Thermogravimetric Analysis (TGA) and Differential Scanning Calorimetry (DSC)

The thermal properties of both polymeric filaments (PLA and TPU) represent a key point in the synthesis of core-shell materials. Due to their direct influence on the final morphology of these materials, the thermal studies were carried out through TGA and DSC analyses (Figures 3 and 4).

In Figure 3a, a complete one-step-degradation of the PLA polymer was noticed between 310 and 390 °C (TGA curves). In the derived TG (DTG) curve, the samples undergo a mass loss of about 98.3% at around 310 °C [14,56]. These results denote a direct dependency—by increasing the temperature, the degree of polymer degradation also increases.

Regarding the DSC curve (Figure 3b), three typical states of thermoplastic polymers, namely the T_g point (glass transition temperature), the T_c point (the point of crystallization) and the T_m point (the melting point), were present [57–59]. During the heating cycle, an endothermic event was observed at around 65 °C, which corresponds to the T_g point. The crystallization point T_c was found around the temperature of 87 °C, and as the temperature increased, a strong endothermic melting process occurred around the temperature of 179 °C [59].

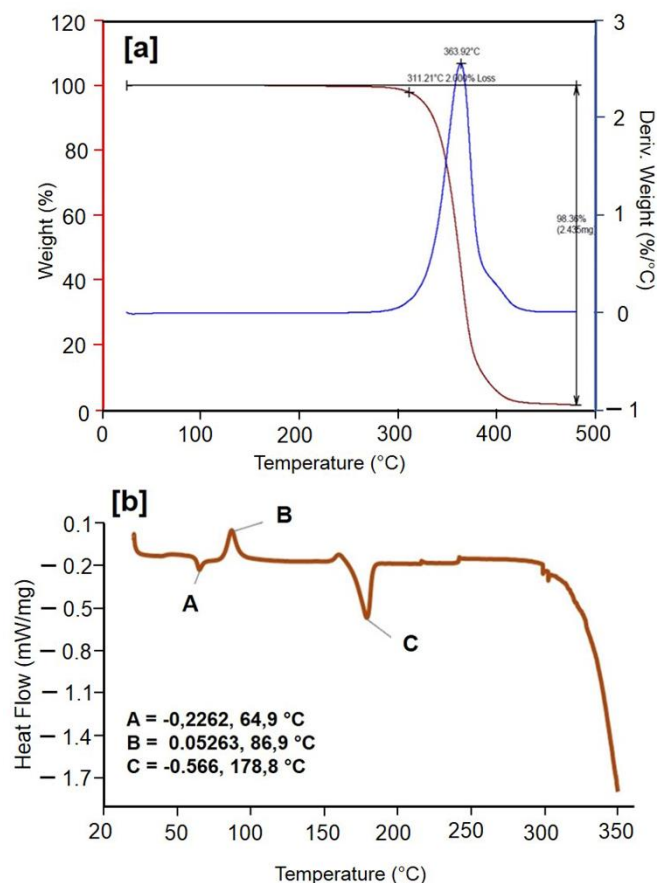


Figure 3. (a) TGA curve of PLA filament; (b) the differential scanning calorimetry (DSC) curve of PLA filament.

Figure 4a presents the TPU thermogram, where a mass loss of 100% was recorded at around 356 °C, suggesting a low thermal stability [60]. The complete degradation of the polymer is accomplished in a

singular step, in the range 380–430 °C. In addition, at lower temperatures, down to 380 °C [61], the DTG curve presents a mass loss of only 2%.

Comparatively to the PLA sample, on the DSC curve of the TPU polymer (Figure 4b), only one endothermic event developed around 165 °C, which is the characteristic temperature of the melting point T_m . In addition, during the temperature rise and after 210 °C, the DSC curve indicates a degradation of the polymer composition [62].

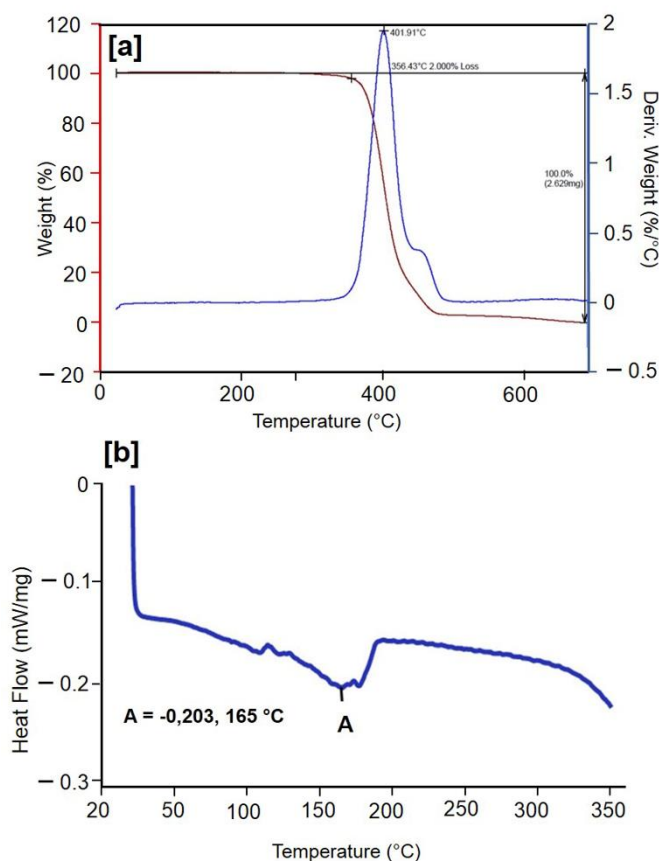


Figure 4. (a) TGA curve of TPU filament; (b) the DSC curve of TPU filament.

3.3. Form Factor Variation

In order to determine the influence of all factors involved in the manufacturing process of these core-shell materials, namely the pressing force, time, and temperature, different investigations were carried out. Firstly, a morphological cross-section analysis of both material types was necessary in order to determine the variation of the form factor, a defining aspect of these materials.

The form factor represents the deviation from the initial cylindrical form of the filaments, up to indefinite and irregular shapes. Due to the incrementally applied pressing force (see Table 1), the cross-section form of the samples becomes more complex and distinct than the ovoid shape present in the case of the reference material (obtained at no pressing force). The maximum and minimum shape measured perpendicular to the longitudinal axis, on each micrograph, were used to explain the degree of deformation. In consequence, x and y axes were chosen according to the preferential direction of deformation, and not as the horizontal and perpendicular to the page.

The experimentally determined deviation from the initial cylindrical shape of the core-shell materials is plotted in Figure 5B, Figure 6B, and Figure 7B. The more the samples' irregularity increases, the lower the values are (from max. value 1.0 corresponding to the reference material down to zero).

Polymeric filaments melt in the feeding hose of commercial 3D printers, after proceeding through a defined route (as can be seen in Figure S2 in the Supplementary Material). Therefore, the cross-section form should be considered a viable and important parameter.

In these terms, it is important to preserve the initial round form of the filament as faithful as possible without being affected by the softening in the HA mass. This aspect ensures its suitability for future additive manufacturing applications [63–65].

In the case of PLA (Figure 5A), at a temperature of 195 °C, the exposure time has a direct influence on the filament shape. With the increase in time, the material begins to deform and at the same time the addition of HA particles increases. The pressing force also influenced the addition of HA particles—as the force increases, the addition of particles increases and the bioceramic coating is formed (Figure S3–Supplementary Material). Similarly, the same temperature does not drastically influence the morphology in a cross-section view of TPU materials, as the initial cylindrical shape is maintained. However, it can be observed that the bioceramic coating is formed when the pressing force increases (see Figure 5A TPU – 60', 120' – $2,5 \times 10^{-4}$ MPa, 5×10^{-4} MPa).

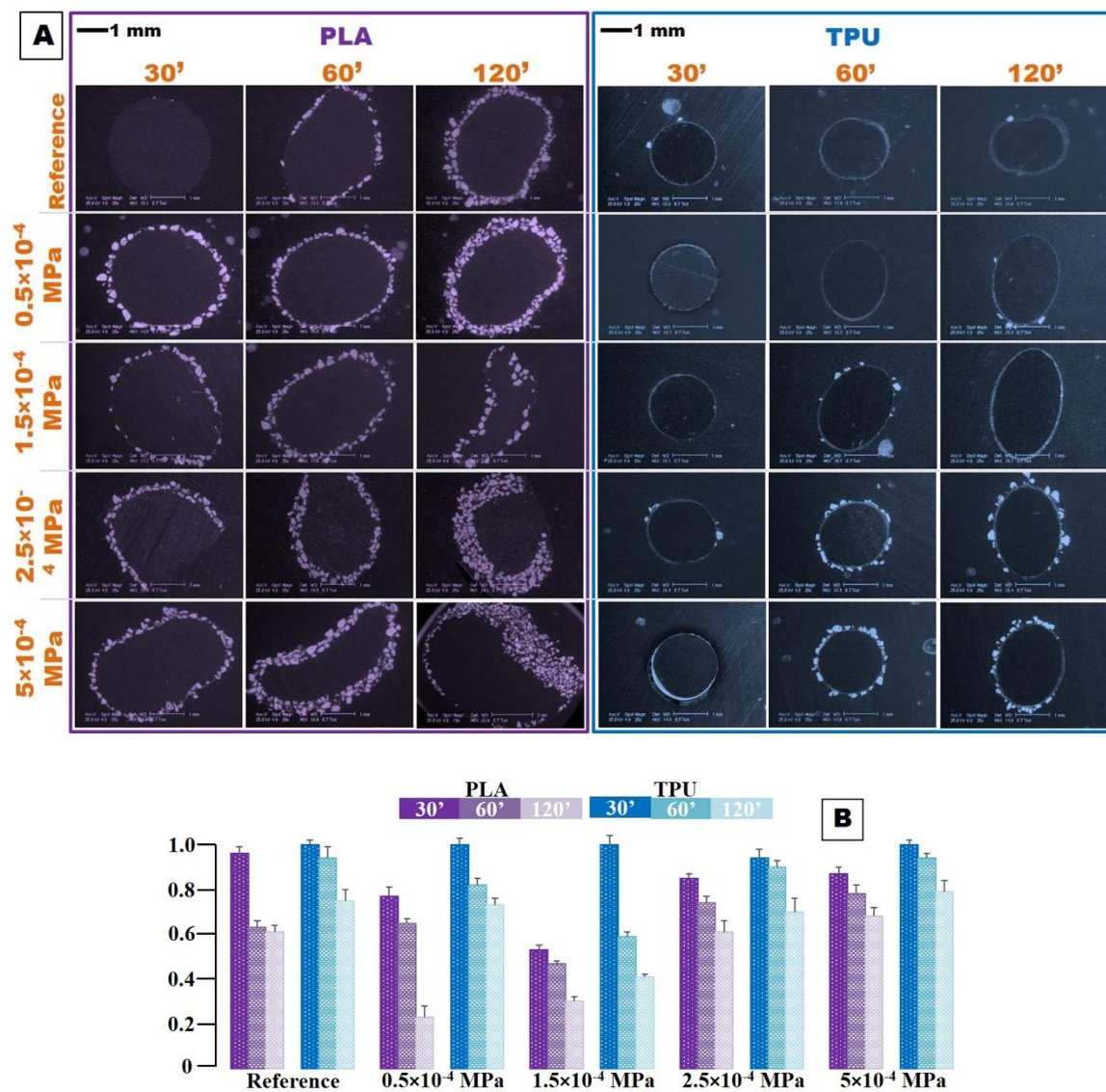


Figure 5. Form factor variation at 195 °C temperature. (A) Section morphology; (B) variation graphs.

In addition, in the case of both PLA and TPU samples, one can note that a uniform or even addition of HA particles causes the cylindricity retention of the polymer filament (see Figure 5A PLA – 30', 60' – 0.5×10^{-4} MPa and TPU – 60' – 2.5×10^{-4} MPa and 60' – 5×10^{-4} MPa).

In order to quantify these variations (Figure 5B), measurements were performed on all of these micrographs. The obtained data were graphically represented for a clear view over the influences of all parameters involved in the technological process. In this regard, i) PLA presents an accentuated variation of the form factor as compared to TPU and ii) the increment of the exposure time is directly proportional to the form factor decrease. At 195 °C, TPU tends to maintain its cylindricity, but as the pressing force increases, the form factor begins to decrease. This is due to the forces and tensions that act upon it.

As the temperature increases, the cross-section morphology changes completely. The micrographs show that, for PLA, the addition of HA particles increases and the cylindricity of the filaments is strongly affected at a higher exposure (see Figure 6A PLA—120'—all pressing forces). This is also highlighted in Figure 6B, where a visible decrease in the form factor of the samples obtained after 120' exposure in the oven can be observed. In addition, at higher pressing forces, the uniform addition of particles increases and the bioceramic coating is well defined, but the filament shape changes to abstract forms (Figure S4—Supplementary material).

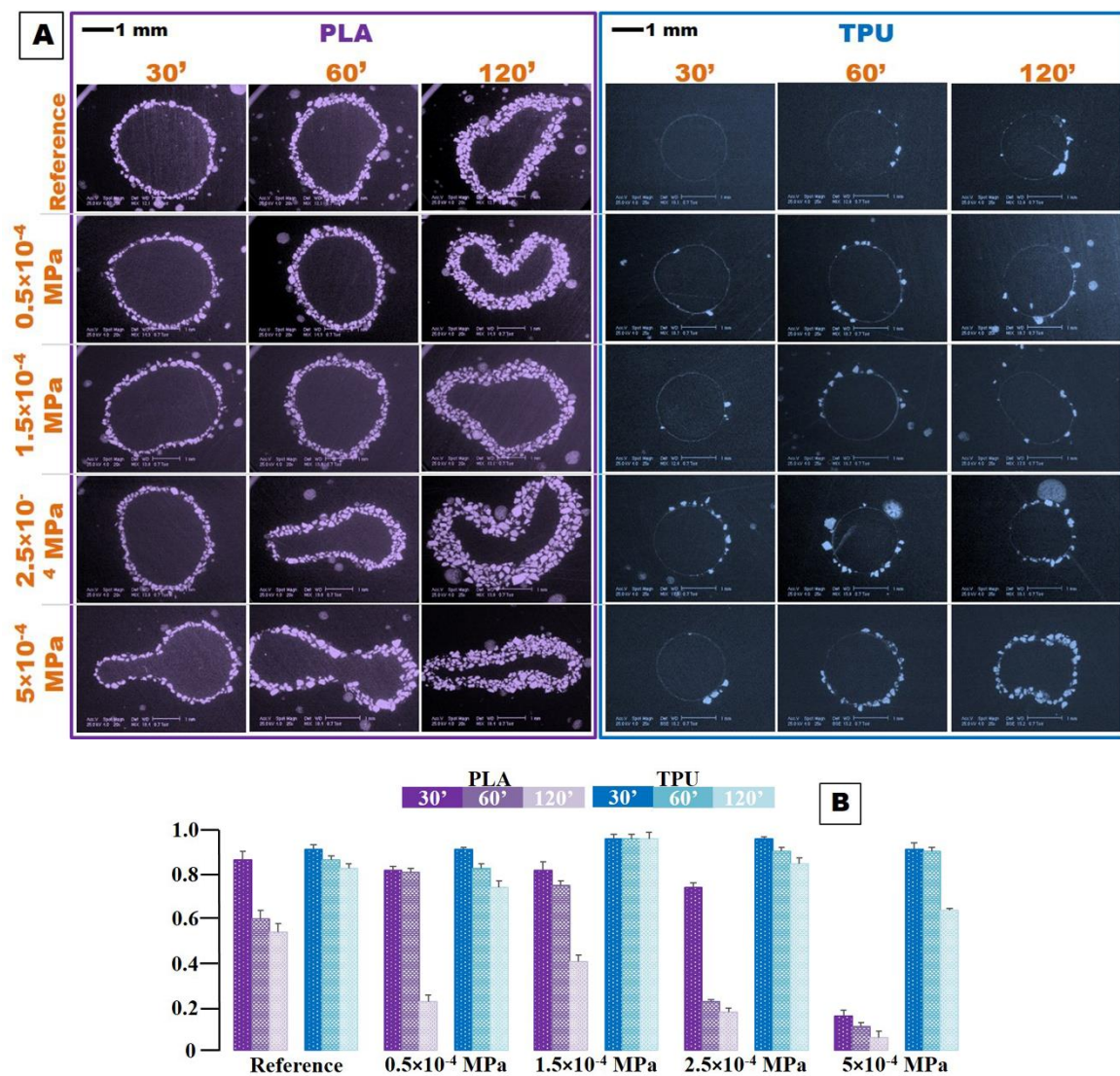


Figure 6. Form factor variation at 205 °C temperature. (A) Section morphology; (B) variation graphs.

Regarding the TPU samples, a 10 °C increased temperature does not significantly influence the addition of HA powder or the initial shape of the filament. In this case, an increased particle addition occurred at higher pressure forces (2.5×10^{-4} MPa and 5×10^{-4} MPa). Figure 6B disclose a tendency to a stable variation of the form factor close to 1 value, which indicates a very small variation in the polymer shape compared to its initial one. When the temperature is increased by another 10 °C, the morphology in the cross-section view reveals major changes. Regarding the PLA (Figure 7A), the filaments' behavior is totally different, slightly chaotic, and cannot be included in a certain pattern. The reference in this case retains its initial shape and also a uniform addition of the particles. Moreover, one can observe that the particles addition increases proportionally with the increase of the exposure time.

Comparatively, in the TPU case, the most visible aspect is related to the addition of HA particles for all investigated samples (Figure S5–Supplementary). In general, these samples retain their cylindricity, but, in this case, it is not possible to discuss a certain visible pattern influenced by the modification of the synthesis parameters, and also the bioceramic coating may not be well defined.

However, the influence of the synthesis parameters' modification was graphically evidenced in terms of form factor variation (Figure 7B). Only in the case of TPU may it be argued that with the increase of the exposure time, the form factor decreases.

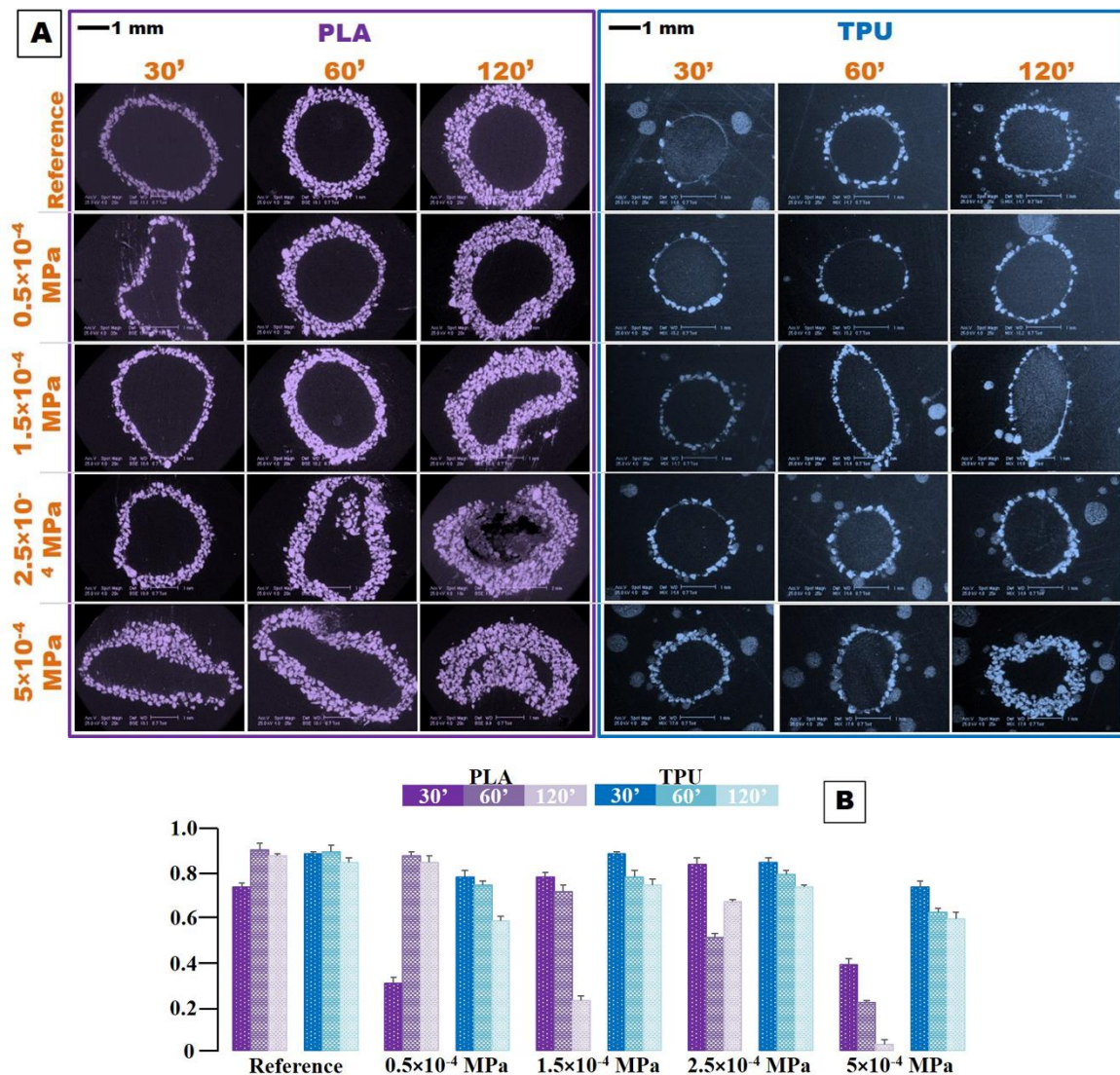


Figure 7. Form factor variation at 215 °C temperature. (A) Section morphology; (B) variation graphs.

3.4. Mass Variation

The mass variation is directly proportional with the addition of HA powder to the surface of the polymeric material and thus with the formation of the bioceramic coating. In the case of PLA filaments, at a temperature of 195 °C, as previously observed in Figure 5A, the materials with the highest amount of powder addition, were the reference ones, regardless of the exposure time. At this temperature, the reference sample displayed the largest mass variation, i.e., 100% (see Figure 8A). Therefore, the mass of the final core-shell material is double that of the initial polymer.

The addition of HA powder to the surface of the TPU filament at 195 °C was slightly diverted as compared to PLA, which is why the mass variation was quite low.

A temperature of 205 °C determined in the case of PLA filaments a good particle addition, directly proportional to both the increment of the exposure time and the increase in the pressing force, as shown in Figure 8B. The final mass of the obtained core-shell materials can vary up to 120% of the initial mass of the polymer, indicating an increased addition of HA powder.

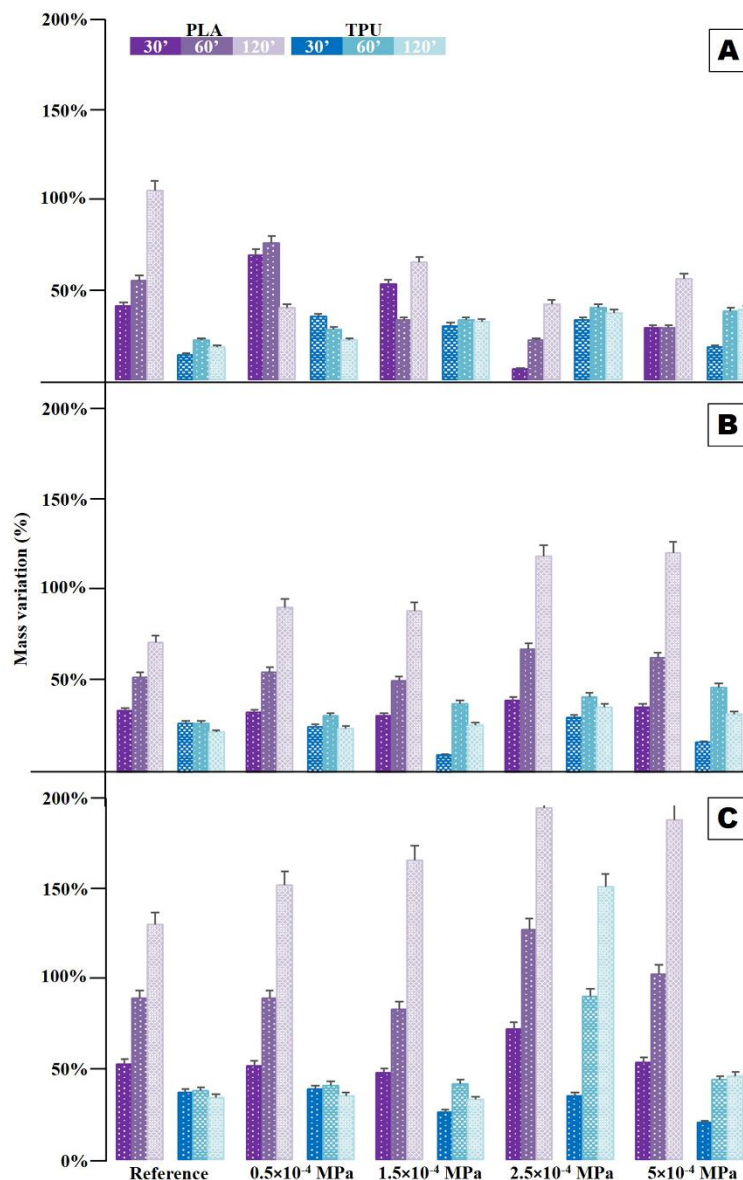


Figure 8. Mass variation at: (A) 195, (B) 205, and (C) 215 °C.

Furthermore, in this case, the addition to the surface of the TPU filament follows the same downtrend, with an unpredictable pattern depending on the parameters' modification. Furthermore, their mass hardly varied—the final mass values were at most 50% higher than those of the initial polymer.

The increased temperature of 215 °C drastically influenced the final mass of the obtained materials. A significant increase in the core-shell materials' mass with a PLA polymer base was recorded. As the exposure time and pressing force increased, their mass increased proportionally, up to 200% values (see Figure 8C).

Moreover, in the case of TPU filaments, significant changes in mass variation were depicted. At this high temperature, the particles adhere easily to the polymer surface, and therefore their mass increases up to 160% at an exposure time of 120'.

3.5. Compression Mechanical Test

To support the preliminary research carried out in this study, the compression strength of the most promising samples (PLA-based materials obtained at 205 °C temperature, an exposure time of 60', and a maximum pressing force of 0.5×10^{-4} MPa, and TPU based materials obtained at 215 °C temperature, 60' of exposure and 2.5×10^{-4} MPa pressing force) was analyzed together with cortical bone tissue.

From the curves of the PLA and TPU filaments with HA insertion (Figure 9), a malleable behavior can be observed, with significant plastic deformation.

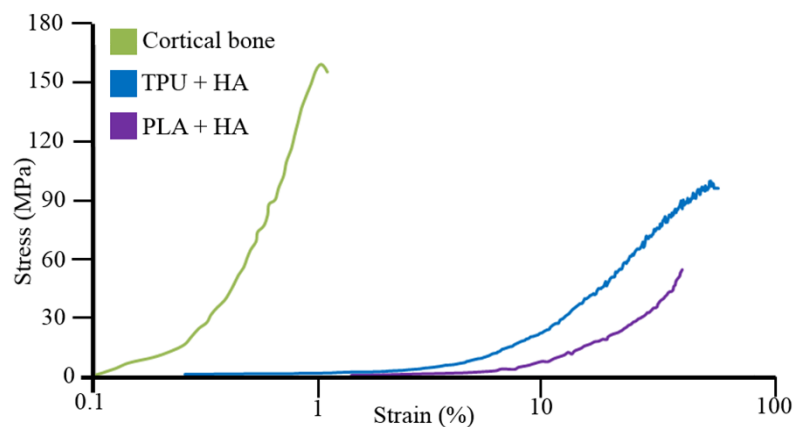


Figure 9. Compression curves of cortical bone, TPU-based materials obtained at 215 °C, 60' of exposure, and 2.5×10^{-4} MPa pressing force with HA particles embedded and PL-based materials obtained at 205 °C, an exposure time of 60', and a maximum pressing force of 0.5×10^{-4} MPa.

In contrast, for compressive loading on cortical bone, rapid hardening occurs after yielding, followed by softening. The bone is considered to be an ideal fragile solid that yields at elasticity limit, which coincides with the compressive strength.

Comparing the compressive strength values of the experimental samples with those of the cortical bone, values of approximately four times smaller than those of the cortical bone in the longitudinal direction were noticed (Table 2). The obtained results show lower values than those of the consecrated metallic materials used in medicine [66–68] but higher than values than those of the ceramic ones [19,69,70].

Table 2. Compressive strength comparison.

Sample	Compression Strength [MPa]
PLA (obtained at 205 °C temperature, 60' exposure time of 60' and 0.5×10^{-4} MPa pressing force)	27.67 ± 3.02
TPU (obtained at 215 °C temperature, 60' exposure time of 60' and 2.5×10^{-4} MPa pressing force)	42.32 ± 2.73
Longitudinal cortical bone	115

3.6. Pull-out Test. Particle Adhesion Strength

The results of the pull-out test performed on the most promising samples (PLA-based materials obtained at 205 °C, for 60', and a maximum pressing force of 0.5×10^{-4} MPa, and TPU based materials obtained at 215 °C, for 60', and a maximum pressing force of 2.5×10^{-4} MPa) are displayed in Figure 10.

The comparative presentation of the PLA and TPU filament curves (Figure 10A) revealed a uniform distribution of deformations with a concentrated loading area at the adhesive–filament interface in the case of PLA samples. In contrast, the deformation of the TPU samples occurred in the incipient part of the filament and was subsequently transferred to the adhesive–filament interface. This uneven behavior can be explained based on the different elasticity modules of the PLA, TPU and the chosen adhesive (the PLA has an elasticity module of approximate three times higher than the adhesive, while the TPU values are close to those of the adhesive) [71–74].

Furthermore, a similar behavior was also depicted for the core-shell materials (Figure 10A). Here, the particles presence changed the state of stresses and deformations, as they were mainly concentrated in the particle coating–adhesive contact region and were gradually transferred to the particle coating–substrate interface. In this case, any particle reorientation/slippage can be encountered, along with the decrease in the assembly rigidity and the displacement increment. Moreover, the breaking occurs at the particle coating–substrate joint and is predominantly cohesive in nature, as particles appear on both adhesive and substrate surface.

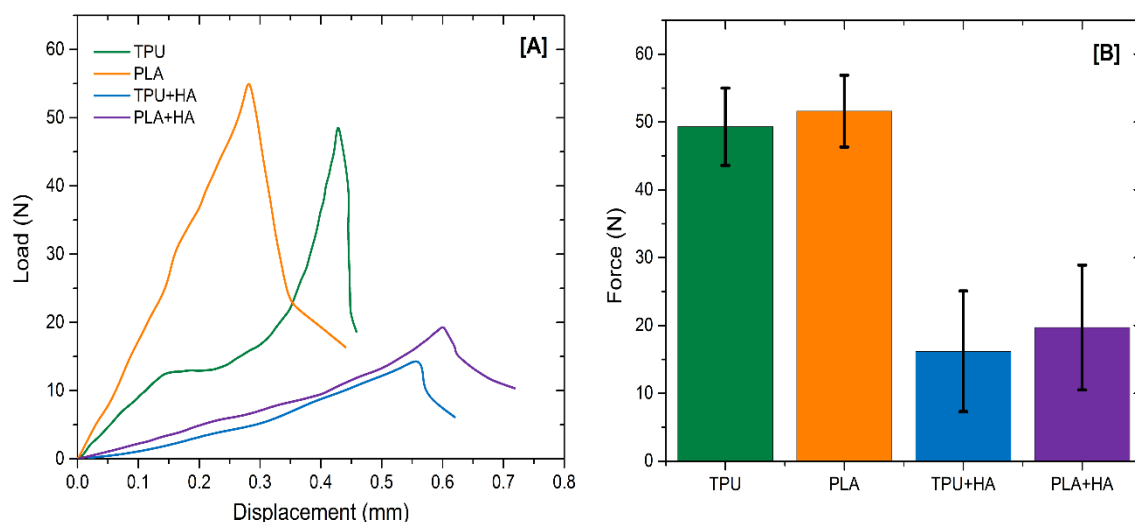


Figure 10. (A) Displacement force curves of TPU, PLA, the TPU-based materials obtained at 215 °C, 60' of exposure, and 2.5×10^{-4} MPa pressing force with HA particles embedded, and PLA-based materials obtained at 205 °C, an exposure time of 60', and a maximum pressing force of 0.5×10^{-4} MPa. (B) The maximum displacement forces for the same samples.

The extraction of the maximum displacement forces' values from Figure 10A was outline in Figure 10B. The obtained results expose a decrease with 61.82% of the displacement force in the

case of PLA-HA coated samples and 67.14% in the case of TPU-HA coated samples, as compared to the displacement forces of blank (as-acquired) polymeric filaments. In respect to both type of coated samples, a large to medium spread of experimental values was reckoned (Figure 10B), which correlates with the SEM investigation's results through the varied particle proportion found at the filament–adhesive interface and also the adhesion/insertion degree of the HA particles.

4. Conclusions

This study targeted the development of a completely new synthesis route for the obtaining of core-shell materials, namely biocompatible polymers coated with bioceramic HA powder. Their manufacturing involved two different types of filaments, PLA and TPU, and the variation of several technological parameters: exposure time and temperature in the electrical oven and the pressing force.

All modifications induced on the working parameters had a direct influence on all the final core-shell materials' properties, especially on their coating.

In this regard, for PLA-based materials, the obtained results recommend a temperature of 205 °C, an exposure time of 60', and a maximum pressing force of 0.5×10^{-4} MPa, as compared to TPU materials for which an increased temperature of 215 °C, 60' of exposure, and higher pressing forces (up to 2.5×10^{-4} MPa) were found adequate because of the *i*) preserved cylindricity of the filament and *ii*) their uniform and well-defined coating. In addition, a comparative study with the cortical bone, of compression resistance, was performed for these samples to demonstrate their applicability in the dentistry and orthopedic fields. These technological parameters hold great promise for an optimum synthesis route of core-shell materials destined for additive manufacturing.

Supplementary Materials: The following are available online at <http://www.mdpi.com/2079-6412/10/3/283/s1>, Figure S1: Schematic representation for the adapted preparation method of the pull-out test samples, Figure S2: Schematic representation of the filament travel route inside of a 3D printer, Figure S3: Form factor variation at 195 °C at higher magnifications, Figure S4: Form factor variation at 205 °C at higher magnifications, Figure S5: Form factor variation at 215 °C temperature at higher magnifications.

Author Contributions: Conceptualization, C.-A.D., F.M. and A.E.C.; Data curation, F.M., A.M.P., R.-C.C. and S.I.V.; Formal analysis, C.-A.D. and F.M.; Funding acquisition, A.M.P.; Investigation, F.M., T.M.B., A.M.P., R.-C.C. and S.I.V.; Methodology, C.-A.D., F.M., A.M.P. and S.I.V.; Project administration, A.M.P.; Resources, C.-A.D., F.M., A.M.P., S.I.V. and L.T.C.; Software, F.M., A.M.P. and S.I.V.; Supervision, F.M. and A.M.P.; Validation, F.M., A.M.P., S.I.V. and L.T.C.; Visualization, C.-A.D., F.M., A.-C.M. and A.M.P.; Writing—original draft, C.-A.D. and A.E.C.; Writing—review & editing, C.-A.D., F.M., A.-C.M., T.M.B. and A.M.P. All authors have read and agreed to the published version of the manuscript.

Funding: This research was funded by the Romanian National Authority for Scientific Research and Innovation, CNCS–UEFISCDI, grant number PN-III-P1-1.1-PD-2016-0761 (contract no. 59/2018).

Conflicts of Interest: Tudor-Mihai Butte is an Assistant Editor for Metals, without access to any information from Coatings.

References

1. Kaya, İ.; Şahin, M.C.; Cingöz, İ.D.; Aydın, N.; Atar, M.; Kizmazoğlu, C.; Kavuncu, S.; Aydın, H.E. Three Dimensional Printing and Biomaterials in the Repairment of Bone Defects; Hydroxyapatite PLA Filaments. *Turk. J. Med. Sci.* **2019**, *49*, 922–927. [[CrossRef](#)] [[PubMed](#)]
2. Niaza, K.; Senatov, F.; Kaloshkin, S.; Maksimkin, A.; Chukov, D. 3D-printed scaffolds based on PLA/HA nanocomposites for trabecular bone reconstruction. *J. Phys. Conf. Ser.* **2016**, *741*, 012068. [[CrossRef](#)]
3. Neacsu, P.; Staras, A.; Voicu, S.; Ionascu, I.; Soare, T.; Uzun, S.; Cojocaru, V.; Pandeale, A.; Croitoru, S.; Miculescu, F. Characterization and in vitro and in vivo assessment of a novel cellulose acetate-coated Mg-based alloy for orthopedic applications. *Materials* **2017**, *10*, 686. [[CrossRef](#)]
4. Ioniță, M.; Crică, L.E.; Voicu, S.I.; Dinescu, S.; Miculescu, F.; Costache, M.; Iovu, H. Synergistic effect of carbon nanotubes and graphene for high performance cellulose acetate membranes in biomedical applications. *Carbohydr. Polym.* **2018**, *183*, 50–61. [[CrossRef](#)]
5. Stan, G.; Popa, A.; Bojin, D. Bioreactivity evaluation in simulated body fluid of magnetron sputtered glass and glass-ceramic coatings: A FTIR spectroscopy study. *Dig. J. Nanomater. Biostructures* **2010**, *5*, 557–566.

6. Ionita, M.; Vasile, E.; Crica, L.E.; Voicu, S.I.; Pandele, A.M.; Dinescu, S.; Predoiu, L.; Galateanu, B.; Hermenean, A.; Costache, M. Synthesis, characterization and in vitro studies of polysulfone/graphene oxide composite membranes. *Compos. Part B Eng.* **2015**, *72*, 108–115. [[CrossRef](#)]
7. Voicu, S.; Pandele, M.; Vasile, E.; Rughinis, R.; Crica, L.; Pilan, L.; Ionita, M. The impact of sonication time through polysulfone-graphene oxide composite films properties. *Dig. J. Nanomater. Biostructures* **2013**, *8*, 1389–1394.
8. Wu, J.; Chen, N.; Bai, F.; Wang, Q. Preparation of poly (vinyl alcohol)/poly (lactic acid)/hydroxyapatite bioactive nanocomposites for fused deposition modeling. *Polym. Compos.* **2018**, *39*, E508–E518. [[CrossRef](#)]
9. Antoniac, I.; Popescu, D.; Zapciu, A.; Antoniac, A.; Miculescu, F.; Moldovan, H. Magnesium Filled Polylactic Acid (PLA) Material for Filament Based 3D Printing. *Materials* **2019**, *12*, 719. [[CrossRef](#)]
10. Stuart, B.W.; Murray, J.W.; Grant, D.M. Two step porosification of biomimetic thin-film hydroxyapatite/alpha-tri calcium phosphate coatings by pulsed electron beam irradiation. *Sci. Rep.* **2018**, *8*, 14530. [[CrossRef](#)]
11. Tite, T.; Popa, A.-C.; Balescu, L.; Bogdan, I.; Pasuk, I.; Ferreira, J.; Stan, G. Cationic Substitutions in Hydroxyapatite: Current Status of the Derived Biofunctional Effects and Their In Vitro Interrogation Methods. *Materials* **2018**, *11*, 2081. [[CrossRef](#)] [[PubMed](#)]
12. Cotrut, C.M.; Vladescu, A.; Dinu, M.; Vranceanu, D.M. Influence of deposition temperature on the properties of hydroxyapatite obtained by electrochemical assisted deposition. *Ceram. Int.* **2018**, *44*, 669–677. [[CrossRef](#)]
13. Vladescu, A.; Cotrut, C.M.; Azem, F.A.; Bramowicz, M.; Pana, I.; Braic, V.; Birlik, I.; Kiss, A.; Braic, M.; Abdulgader, R. Sputtered Si and Mg doped hydroxyapatite for biomedical applications. *Biomed. Mater.* **2018**, *13*, 025011. [[CrossRef](#)]
14. Matos, B.D.M.; Rocha, V.; da Silva, E.J.; Moro, F.H.; Bottene, A.C.; Ribeiro, C.A.; dos Santos Dias, D.; Antonio, S.G.; do Amaral, A.C.; Cruz, S.A. Evaluation of commercially available polylactic acid (PLA) filaments for 3D printing applications. *J. Therm. Anal. Calorim.* **2019**, *137*, 555–562. [[CrossRef](#)]
15. Manganiello, C.; Naso, D.; Cupertino, F.; Fiume, O.; Percoco, G. Investigating the Potential of Commercial-Grade Carbon Black-Filled TPU for the 3D Printing of Compressive Sensors. *Micromachines* **2019**, *10*, 46. [[CrossRef](#)]
16. Haryńska, A.; Gubanska, I.; Kucinska-Lipka, J.; Janik, H. Fabrication and Characterization of Flexible Medical-Grade TPU Filament for Fused Deposition Modeling 3DP Technology. *Polymers* **2018**, *10*, 1304. [[CrossRef](#)]
17. Miculescu, F.; Miculescu, M.; Ciocan, L.; Ernuteanu, A.; Antoniac, I.; Pencea, I.; Matei, E. Comparative studies regarding heavy elements concentration in human cortical bone. *Dig. J. Nanomater. Biostructures* **2011**, *6*, 1117–1127.
18. Miculescu, F.; Stan, G.; Ciocan, L.; Miculescu, M.; Berbecaru, A.; Antoniac, I. Cortical bone as resource for producing biomimetic materials for clinical use. *Dig. J. Nanomater. Biostructures* **2012**, *7*, 1667–1677.
19. Miculescu, F.; Mocanu, A.C.; Stan, G.E.; Miculescu, M.; Maidaniuc, A.; Cîmpean, A.; Mitran, V.; Voicu, S.I.; Machedon-Pisu, T.; Ciocan, L.T. Influence of the modulated two-step synthesis of biogenic hydroxyapatite on biomimetic products' surface. *Appl. Surf. Sci.* **2018**, *438*, 147–157. [[CrossRef](#)]
20. Maidaniuc, A.; Miculescu, F.; Voicu, S.I.; Andronescu, C.; Miculescu, M.; Matei, E.; Mocanu, A.C.; Pencea, I.; Csaki, I.; Machedon-Pisu, T. Induced wettability and surface-volume correlation of composition for bovine bone derived hydroxyapatite particles. *Appl. Surf. Sci.* **2018**, *438*, 158–166. [[CrossRef](#)]
21. Cicala, G.; Giordano, D.; Tosto, C.; Filippone, G.; Recca, A.; Blanco, I. Polylactide (PLA) filaments a biobased solution for additive manufacturing: Correlating rheology and thermomechanical properties with printing quality. *Materials* **2018**, *11*, 1191. [[CrossRef](#)]
22. Corcione, C.E.; Scalera, F.; Gervaso, F.; Montagna, F.; Sannino, A.; Maffezzoli, A. One-step solvent-free process for the fabrication of high loaded PLA/HA composite filament for 3D printing. *J. Therm. Anal. Calorim.* **2018**, *134*, 575–582. [[CrossRef](#)]
23. Popescu, D.; Zapciu, A.; Amza, C.; Baciu, F.; Marinescu, R. FDM process parameters influence over the mechanical properties of polymer specimens: A review. *Polym. Test.* **2018**, *69*, 157–166. [[CrossRef](#)]
24. Motaparti, K.P.; Taylor, G.; Leu, M.C.; Chandrashekhara, K.; Castle, J.; Matlack, M. Experimental investigation of effects of build parameters on flexural properties in fused deposition modelling parts. *Virtual Phys. Prototyp.* **2017**, *12*, 207–220. [[CrossRef](#)]

25. Zaldivar, R.; Witkin, D.; McLouth, T.; Patel, D.; Schmitt, K.; Nokes, J. Influence of processing and orientation print effects on the mechanical and thermal behavior of 3D-Printed ULTEM@9085 Material. *Addit. Manuf.* **2017**, *13*, 71–80. [[CrossRef](#)]
26. Tanikella, N.G.; Wittbrodt, B.; Pearce, J.M. Tensile strength of commercial polymer materials for fused filament fabrication 3D printing. *Addit. Manuf.* **2017**, *15*, 40–47. [[CrossRef](#)]
27. McLouth, T.D.; Severino, J.V.; Adams, P.M.; Patel, D.N.; Zaldivar, R.J. The impact of print orientation and raster pattern on fracture toughness in additively manufactured ABS. *Addit. Manuf.* **2017**, *18*, 103–109. [[CrossRef](#)]
28. Yu, L.Y.; Zhu, B.; Cai, X.; Wang, Y.W.; Han, R.H.; Li, Y.W. Review of polymer surface modification method. *Mater. Sci. Forum* **2016**, *852*, 626–631. [[CrossRef](#)]
29. Ozeki, K.; Hirakuri, K. The effect of nitrogen and oxygen plasma on the wear properties and adhesion strength of the diamond-like carbon film coated on PTFE. *Appl. Surf. Sci.* **2008**, *254*, 1614–1621. [[CrossRef](#)]
30. Desmet, T.; Morent, R.; De Geyter, N.; Leys, C.; Schacht, E.; Dubruel, P. Nonthermal plasma technology as a versatile strategy for polymeric biomaterials surface modification: A review. *Biomacromolecules* **2009**, *10*, 2351–2378. [[CrossRef](#)]
31. Bielawski, M.; Beres, W. FE modelling of surface stresses in erosion-resistant coatings under single particle impact. *Wear* **2007**, *262*, 167–175. [[CrossRef](#)]
32. van Kampen, A.; Kohlus, R. Statistical modelling of coating layer thickness distributions: Influence of overspray on coating quality. *Powder Technol.* **2018**, *325*, 557–567. [[CrossRef](#)]
33. Bogdanovich, V.; Giorbelidze, M. Mathematical modelling of powder material motion and transportation in high-temperature flow core during plasma coatings application. *IOP Conf. Ser. Mater. Sci. Eng.* **2018**, *327*, 022036. [[CrossRef](#)]
34. Dyshlovenko, S.; Pawlowski, L.; Pateyron, B.; Smurov, I.; Harding, J. Modelling of plasma particle interactions and coating growth for plasma spraying of hydroxyapatite. *Surf. Coat. Technol.* **2006**, *200*, 3757–3769. [[CrossRef](#)]
35. Riau, A.K.; Mondal, D.; Setiawan, M.; Palaniappan, A.; Yam, G.H.; Liedberg, B.; Venkatraman, S.S.; Mehta, J.S. Functionalization of the polymeric surface with bioceramic nanoparticles via a novel, nonthermal dip coating method. *ACS Appl. Mater. Interfaces* **2016**, *8*, 35565–35577. [[CrossRef](#)]
36. Li, T.-T.; Ling, L.; Lin, M.-C.; Jiang, Q.; Lin, Q.; Lin, J.-H.; Lou, C.-W. Properties and mechanism of hydroxyapatite coating prepared by electrodeposition on a braid for biodegradable bone scaffolds. *Nanomaterials* **2019**, *9*, 679. [[CrossRef](#)]
37. Corcione, C.E.; Gervaso, F.; Scalera, F.; Montagna, F.; Maiullaro, T.; Sannino, A.; Maffezzoli, A. 3D printing of hydroxyapatite polymer-based composites for bone tissue engineering. *J. Polym. Eng.* **2017**, *37*, 741–746. [[CrossRef](#)]
38. Petrovskaya, T.; Toropkov, N.; Mironov, E.; Azarmi, F. 3D printed biocompatible polylactide-hydroxyapatite based material for bone implants. *Mater. Manuf. Process.* **2018**, *33*, 1899–1904. [[CrossRef](#)]
39. Dudin, S.; Cotrut, C.M.; Dinu, M.; Zykova, A.; Parau, A.C.; Yakovin, S.; Vladescu, A. Comparative study of the hydroxyapatite coatings prepared with/without substrate bias. *Ceram. Int.* **2017**, *43*, 14968–14975. [[CrossRef](#)]
40. Miculescu, F.; Jepu, I.; Porosnicu, C.; Lungu, C.; Miculescu, M.; Burhala, B. A study on the influence of the primary electron beam on nanodimensional layers analysis. *Dig. J. Nanomater. Biostructures* **2011**, *6*, 335–345.
41. Miculescu, F.; Ciocan, L.; Miculescu, M.; Ernuteanu, A. Effect of heating process on micro structure level of cortical bone prepared for compositional analysis. *Dig. J. Nanomater. Biostructures* **2011**, *6*, 225–233.
42. Akindoyo, J.O.; Beg, M.; Ghazali, S.; Islam, M.; Jeyaratnam, N.; Yuvaraj, A. Polyurethane types, synthesis and applications—A review. *RSC Adv.* **2016**, *6*, 114453–114482. [[CrossRef](#)]
43. Ahmed, J.; Varshney, S.K. Polylactides—chemistry, properties and green packaging technology: A review. *Int. J. Food Prop.* **2011**, *14*, 37–58. [[CrossRef](#)]
44. Mocanu, A.-C.; Stan, G.E.; Maidaniuc, A.; Miculescu, M.; Antoniac, I.V.; Ciocoiu, R.-C.; Voicu, S.I.; Mitran, V.; Cîmpean, A.; Miculescu, F. Naturally-derived biphasic calcium phosphates through increased phosphorus-based reagent amounts for biomedical applications. *Materials* **2019**, *12*, 381. [[CrossRef](#)]
45. Maidaniuc, A.; Miculescu, M.; Voicu, S.; Ciocan, L.; Niculescu, M.; Corobea, M.; Rada, M.; Miculescu, F. Effect of micron sized silver particles concentration on the adhesion induced by sintering and antibacterial properties of hydroxyapatite microcomposites. *J. Adhes. Sci. Technol.* **2016**, *30*, 1829–1841. [[CrossRef](#)]

46. Miculescu, F.; Maidaniuc, A.; Stan, G.; Miculescu, M.; Voicu, S.; Cimpean, A.; Mitran, V.; Batalu, D. Tuning hydroxyapatite particles' characteristics for solid freeform fabrication of bone scaffolds. In *Advanced Composite Materials*; Tiwari, A., Alenezi, M.R., Jun, S.C., Eds.; John Wiley & Sons: Hoboken, NJ, USA, 2016; pp. 321–397. ISBN 978-111-924-286-4.
47. Stabile, L.; Scungio, M.; Buonanno, G.; Arpino, F.; Ficco, G. Airborne particle emission of a commercial 3D printer: The effect of filament material and printing temperature. *Indoor Air* **2017**, *27*, 398–408. [[CrossRef](#)]
48. van Manen, T.; Janbaz, S.; Zadpoor, A.A. Programming 2D/3D shape-shifting with hobbyist 3D printers. *Mater. Horiz.* **2017**, *4*, 1064–1069. [[CrossRef](#)]
49. ASTM:C633. *Standard Test Method for Adhesion or Cohesion Strength of Thermal Spray Coatings*; ASTM International: West Conshohocken, PA, USA, 2008.
50. Liu, D.-M.; Yang, Q.; Troczynski, T. Sol-gel hydroxyapatite coatings on stainless steel substrates. *Biomaterials* **2002**, *23*, 691–698. [[CrossRef](#)]
51. Zhang, S.; Wang, Y.; Zeng, X.; Khor, K.A.; Weng, W.; Sun, D. Evaluation of adhesion strength and toughness of fluoridated hydroxyapatite coatings. *Thin Solid Films* **2008**, *516*, 5162–5167. [[CrossRef](#)]
52. Cheng, K.; Ren, C.; Weng, W.; Du, P.; Shen, G.; Han, G.; Zhang, S. Bonding strength of fluoridated hydroxyapatite coatings: A comparative study on pull-out and scratch analysis. *Thin Solid Films* **2009**, *517*, 5361–5364. [[CrossRef](#)]
53. Stan, G.; Morosanu, C.; Marcov, D.; Pasuk, I.; Miculescu, F.; Reumont, G. Effect of annealing upon the structure and adhesion properties of sputtered bio-glass/titanium coatings. *Appl. Surf. Sci.* **2009**, *255*, 9132–9138. [[CrossRef](#)]
54. Ozeki, K.; Masuzawa, T.; Aoki, H. Fabrication of hydroxyapatite thin films on polyetheretherketone substrates using a sputtering technique. *Mater. Sci. Eng. C* **2017**, *72*, 576–582. [[CrossRef](#)] [[PubMed](#)]
55. Borie, E.; Rosas, E.; Kuramochi, G.; Etcheberry, S.; Olate, S.; Weber, B. Oral Applications of Cyanoacrylate Adhesives: A Literature Review. *BioMed Res. Int.* **2019**, *2019*, 8217602. [[CrossRef](#)]
56. Wady, P.; Wasilewski, A.; Brock, L.; Edge, R.; Baidak, A.; McBride, C.; Leay, L.; Griffiths, A.; Vallés, C. Effect of ionising radiation on the mechanical and structural properties of 3D printed plastics. *Addit. Manuf.* **2020**, *31*, 100907. [[CrossRef](#)]
57. Polonio-Alcalá, E.; Rabionet, M.; Gallardo, X.; Angelats, D.; Ciurana, J.; Ruiz-Martínez, S.; Puig, T. PLA Electrospun Scaffolds for Three-Dimensional Triple-Negative Breast Cancer Cell Culture. *Polymers* **2019**, *11*, 916. [[CrossRef](#)]
58. Lee, J.; Lee, H.; Cheon, K.-H.; Park, C.; Jang, T.-S.; Kim, H.-E.; Jung, H.-D. Fabrication of poly (lactic acid)/Ti composite scaffolds with enhanced mechanical properties and biocompatibility via fused filament fabrication (FFF)-based 3D printing. *Addit. Manuf.* **2019**, *30*, 100883. [[CrossRef](#)]
59. Liu, Y.; Zhang, W.; Zhang, F.; Leng, J.; Pei, S.; Wang, L.; Jia, X.; Cotton, C.; Sun, B.; Chou, T.-W. Microstructural design for enhanced shape memory behavior of 4D printed composites based on carbon nanotube/poly(lactic acid) filament. *Compos. Sci. Technol.* **2019**, *181*, 107692. [[CrossRef](#)]
60. Xie, J.; Zhai, X.; Hse, C.; Shupe, T.; Pan, H. Polyols from microwave liquefied bagasse and its application to rigid polyurethane foam. *Materials* **2015**, *8*, 8496–8509. [[CrossRef](#)]
61. Kanabenta, W.; Potiyaraj, P. Graphene/Thermoplastic Polyurethane Composites. In *Key Engineering Materials*; Trans Tech Publications Ltd.: Stafa-Zurich, Switzerland, 2018; Volume 773, pp. 77–81.
62. Marycz, K.; Marek, M.; Grzesiak, J.; Lis, A.; Śmieszek, A. Biphasic polyurethane/poly(lactide) sponges doped with nano-hydroxyapatite (nHA) combined with human adipose-derived mesenchymal stromal stem cells for regenerative medicine applications. *Polymers* **2016**, *8*, 339. [[CrossRef](#)]
63. Chen, Q.; Cao, P.F.; Advincula, R.C. Mechanically robust, ultraelastic hierarchical foam with tunable properties via 3D printing. *Adv. Funct. Mater.* **2018**, *28*, 1800631. [[CrossRef](#)]
64. Wu, G.; Liu, S.; Jia, H.; Dai, J. Preparation and properties of heat resistant poly(lactic acid) (PLA)/nano-SiO₂ composite filament. *J. Wuhan. Univ. Technol.* **2016**, *31*, 164–171. [[CrossRef](#)]
65. Chacón, J.; Caminero, M.A.; García-Plaza, E.; Núñez, P.J. Additive manufacturing of PLA structures using fused deposition modelling: Effect of process parameters on mechanical properties and their optimal selection. *Mater. Des.* **2017**, *124*, 143–157. [[CrossRef](#)]
66. Parthasarathy, J.; Starly, B.; Raman, S.; Christensen, A. Mechanical evaluation of porous titanium (Ti6Al4V) structures with electron beam melting (EBM). *J. Mech. Behav. Biomed. Mater.* **2010**, *3*, 249–259. [[CrossRef](#)]

67. Cheng, X.; Li, S.; Murr, L.; Zhang, Z.; Hao, Y.; Yang, R.; Medina, F.; Wicker, R. Compression deformation behavior of Ti–6Al–4V alloy with cellular structures fabricated by electron beam melting. *J. Mech. Behav. Biomed. Mater.* **2012**, *16*, 153–162. [[CrossRef](#)]
68. Barriuso, S.; Chao, J.; Jiménez, J.A.; García, S.; González-Carrasco, J.L. Fatigue behavior of Ti6Al4V and 316 LVM blasted with ceramic particles of interest for medical devices. *J. Mech. Behav. Biomed. Mater.* **2014**, *30*, 30–40. [[CrossRef](#)]
69. Mocanu, A.-C.; Miculescu, M.; Machedon-Pisu, T.; Maidaniuc, A.; Ciocoiu, R.C.; Ioniță, M.; Pasuk, I.; Stan, G.E.; Miculescu, F. Internal and external surface features of newly developed porous ceramics with random interconnected 3D channels by a fibrous sacrificial porogen method. *Appl. Surf. Sci.* **2019**, *489*, 226–238. [[CrossRef](#)]
70. Beltrán-Fernández, J.A.; Hernandez-Gomez, L.H.; Rodriguez-Cañizo, R.G.; Urriolagoitia-Calderón, G.; Urriolagoitia-Sosa, G.; González-Rebatú, A.; Dufoo-Olvera, M. Mechanical behavior of a calcium phosphate ceramic bone graft used in the rehabilitation of a C4 human vertebra. *Appl. Mech. Mater.* **2007**, *7*, 101–106. [[CrossRef](#)]
71. Pastor-Artigues, M.-M.; Roure-Fernández, F.; Ayneto-Gubert, X.; Bonada-Bo, J.; Pérez-Guindal, E.; Buj-Corral, I. Elastic Asymmetry of PLA Material in FDM-Printed Parts: Considerations Concerning Experimental Characterisation for Use in Numerical Simulations. *Materials* **2020**, *13*, 15. [[CrossRef](#)]
72. He, J.Y.; Ding, Y.M.; Xue, Z.C.; Yang, W.M. Research on the Elasticity Modulus of Short Glass Fiber/Thermoplastic Polyurethane (SGF-TPU) Composites. In *Key Engineering Materials*; Trans Tech Publications Ltd.: Stafa-Zurich, Switzerland, 2013; Volume 561, pp. 152–157.
73. Chen, C.-C.; Chueh, J.-Y.; Tseng, H.; Huang, H.-M.; Lee, S.-Y. Preparation and characterization of biodegradable PLA polymeric blends. *Biomaterials* **2003**, *24*, 1167–1173. [[CrossRef](#)]
74. Tripodo, G.; Wischke, C.; Lendlein, A. Highly Flexible Poly (ethyl-2-cyanoacrylate) Based Materials Obtained by Incorporation of Oligo (ethylene glycol) diglycidylether. *Macromol. Symp.* **2011**, *309*, 49–58. [[CrossRef](#)]



© 2020 by the authors. Licensee MDPI, Basel, Switzerland. This article is an open access article distributed under the terms and conditions of the Creative Commons Attribution (CC BY) license (<http://creativecommons.org/licenses/by/4.0/>).